Article

Not peer-reviewed version

3D Bioprinting of Alginate-Based Hydrogels to Investigate Osteogenic Differentiation of hBMSCS In Vitro

Ana Catarina Sousa , Grace Mcdermott , Fraser Shields , Rui Alvites , Bruna Lopes , Patrícia Sousa , Alícia Moreira , André Coelho , José Domingos Santos , Luís Atayde , Nuno Alves , Stephen Richardson , Marco Domingos , Ana Colette Maurício *

Posted Date: 24 October 2024

doi: 10.20944/preprints202410.1926.v1

Keywords: alginate; bioInk; bioprinting; bone regeneration; collagen; hydroxyapatite; human bone marrow stem/stromal cells

Article

3D Bioprinting of Alginate-Based Hydrogels to Investigate Osteogenic Differentiation of hBMSCS *In Vitro*

Ana Catarina Sousa [1,2,3], Grace Mcdermott [4], Fraser Shields [4], Rui Alvites [1,2,3,5], Bruna Lopes [1,2,3], Patrícia Sousa [1,2,3], Alícia Moreira [1,2,3], André Coelho [1,2,3], José Domingos Santos [6], Luís Atayde [1,2,3], Nuno Alves [7], Stephen Richardson [4], Marco Domingos [8] and Ana Colette Maurício [1,2,3,*]

1 Departamento de Clínicas Veterinárias, Instituto de Ciências Biomédicas de Abel Salazar (ICBAS), Universidade do Porto (UP), Rua de Jorge Viterbo Ferreira, nº 228, 4050-313 Porto, Portugal
2 Centro de Estudos de Ciência Animal (CECA), Instituto de Ciências, Tecnologias e Agroambiente da Universidade do Porto (ICETA), Rua D. Manuel II, Apartado 55142, 4051-401, Porto, Portugal;
3 Associate Laboratory for Animal and Veterinary Science (AL4AnimalS), Lisboa, Portugal.
4 Department of Cell Matrix Biology & Regenerative Medicine, Faculty of Biology, Medicine & Health, The University of Manchester, Manchester M13 9PL, UK
5 Instituto Universitário de Ciências da Saúde (CESPU), Avenida Central de Gandra 1317, Gandra, 4585-116 Paredes, Portugal.
6 REQUIMTE-LAQV, Departamento de Engenharia Metalúrgica e Materiais, Faculdade de Engenharia, UP
7 Centre for Rapid and Sustainable Product Development (CDRSP), Polytechnic Institute of Leiria, Portugal
8 Department of Mechanical and Aerospace Engineering, School of Engineering, Faculty of Science and Engineering & Henry Royce Institute, The University of Manchester, Manchester M13 9PL, UK
* Correspondence: ana.colette@hotmail.com or acmauricio@icbas.up.pt (A.C.M.)

Abstract: Three-dimensional (3D) models with improved biomimicry are essential to reduce animal experimentation and drive innovation in tissue engineering. In this study, we investigate the use of alginate-based materials as polymeric inks for 3D bioprinting of osteogenic models using human bone marrow stem/stromal cells (hBMSCs). A composite bioink incorporating alginate, nano-hydroxyapatite (nHA), type I collagen (Col) and hBMSCs was developed and for extrude-based printing. Rheological tests perfomed on crosslinked hydrogels confirm the formation of solid-like structures, consistently indicating a superior storage modulus in relation to the loss modulus. The swelling behaviour analysis showed that the addition of Col and nHA into an alginate matrix can enhance the swelling rate of the resulting composite hydrogels, which maximizes cell proliferation within the structure. The LIVE/DEAD assay outcomes demonstrate that the inclusion of nHA and Col did not detrimentally affect the viability of hBMSCs over seven days post-printing. PrestoBlue™ revealed a higher hBMSCs viability in the alginate-nHA-Col hydrogel compared to the remaining groups. Gene expression analysis revealed that alginate-nHA-col bioink favoured a higher expression of osteogenic markers, including secreted phosphoprotein-1 (SPP1) and collagen type 1 alpha 2 chain (COL1A2), in hBMSCs after 14 days, indicating the pro-osteogenic differentiation potential of the hydrogel. This study demonstrates that the incorporation of nHA and Col into alginate enhances osteogenic potential and therefore provides a bioprinted model to systematically study osteogenesis and the early stages of tissue maturation *in vitro*.

Keywords: alginate; bioInk; bioprinting; bone regeneration; collagen; hydroxyapatite; human bone marrow stem/stromal cells

1. Introduction

Bone diseases are an important global public health problem that have significant economic effects, particularly for people suffering from osteoporosis [1–3]. Research models that replicate the bone structure, its functions, the cell-cell and cell-matrix interactions that occur *in vivo* have been

 doi:10.20944/preprints202410.1926.v1

developed to ensure the clinical translation of new treatments to more reliably treat these bone pathologies [4]. Considering ever-increasing growth of bone tissue engineering and the challenge of bone's complexity, in the last decade, several three-dimensional (3D) models have been developed to mimic the bone microenvironment aiming to reduce or replace the dependence on animal experiments [5]. Nevertheless, these models are unable to fully replicate the complex structural and cellular composition of bone tissue [6].

Bioprinting has emerged as a transformative approach within regenerative medicine and tissue engineering, demonstrating significant potential for the generation of three-dimensional tissue constructs [7]. A noteworthy application of this technology is in the field of bone tissue regeneration, which has been increasingly emphasized. This is mainly due to the structural and biological complexities that define the nature of bone tissue [8]. The production of 3D models of bone tissue remains a major challenge to achieve, since the selection of materials, manufacturing processes and the establishment of optimal conditions to support multiple cell populations, as well as their osteodifferentiation, leads to the development of these models not being a trivial task [9]. The choice of biocompatible materials plays an important role not only in mimicking the physical properties of bone, although it also provides the biochemical pathways necessary to guide the behavior of stem cells. Various biomaterials, such as calcium phosphate ceramics, bioactive glass and hydrogels (e.g., alginate), have been used in bioprinting to promote osteogenesis.

Alginate, an FDA-approved natural polysaccharide, is widely employed in biomedical applications as a bioink [10,11]. This widespread use is attributed to its low cost [12], accessibility [13], and ease of preparation [14]. Consequently, alginate-based hydrogels emerge as a promising candidate capable of offering a three-dimensional (3D) microenvironment encompassing both organic and inorganic elements vital for osteoblast functionality. Nevertheless, alginate is an inert material and lacks osteoinductive signals necessary for promoting osteoblast differentiation and bone formation. To address these limitations, additional modifications are required to enhance its osteogenic potential. Combining alginate with collagen (Col), the primary structural component of the extracellular matrix (ECM), and bioactive ceramics, such as hydroxyapatite (HA), can significantly increase osteoconductivity [12,15,16]. These materials were selected due to bone's hierarchical structure, consisting of living cells immersed in a matrix primarily composed of Col and HA [17]. Researchers focus on mimicking the bone's composition to achieve a high degree of similarity between the 3D printed scaffold and bone tissue. Col represents nearly 80% of the organic material in bones [18,19]. It is a suitable biomaterial due to its outstanding biocompatibility, degradability, adhesion characteristics, osteogenic induction properties, and minimal immunogenicity [20].Additionally, nano-HA (nHA) presents stability, biocompatibility, hydrophilicity, and degradability. This ceramic enhances the adhesion and proliferation of osteoblasts and possesses the capacity to establish chemical bonds with the surrounding bone tissue [21]. The combination of alginate, a biocompatible polymer capable of forming stable gels, nHA, an osteoconductive element, and Col, a primary organic component of natural bone, has been demonstrated to improve the biomineralization, promoting natural bone regeneration [22]. These biomaterials have been utilized in bone bioprinting applications to replicate the complex hierarchical structure of bone tissue, which is essential for its biological functions [23–26]. Hassani *et al.* developed cell-laden alginate-nHA-Col microcapsules for modular bone tissue and the results suggest that this structure promotes mineralization and the osteogenesis signaling pathways of the encapsulated cells [27]. Despite their effectiveness in creating controlled microenvironments for osteogenesis, microcapsules present certain limitations. They are unable to fully replicate the complex hierarchical structure of native bone tissue, as cell-material interactions are restricted by the encapsulation process within the alginate matrix. This confinement limits the degree of cell-matrix interaction, potentially hindering cellular behaviors such as migration and differentiation. Additionally, microcapsules present challenges in reproducibility, as their size, composition, and cell distribution can differ. In contrast, bioprinting techniques using the same materials offer advantages in creating more structured, complex 3D environments that more closely mimic native bone architecture. These methods enable enhanced cell-matrix interactions, which can improve osteogenesis. Furthermore, the

 doi:10.20944/preprints202410.1926.v1

automation and standardization of biofabrication processes, provides greater reproducibility of 3D tissue models.

In the field of regenerative medicine, the integration of biomaterials with mesenchymal stem/stromal cells (MSCs) has been prevalent, as this approach promotes the proliferation and differentiation of MSCs [28,29].These cells can be isolated from several tissues, including bone marrow [30]. Human MSCs derived from bone marrow (hBMSCs) are considered multipotent stromal cells and they possess the inherent capacity to differentiate into osteoblasts and form bone tissue, allowing their osteogenic differentiation to be studied directly in a 3D environment [31,32].

In light of these considerations, the present study aimed to develop a bioink formulation tailored for extrusion-based bioprinting, incorporating alginate, nHA, and Col, along with hBMSCs. This is the first study applying these biomaterials and hBMSCs, through biofabrication (using a pressure-assisted extrusion technique), seeking to address the fundamental challenge of replicating the composition of the native ECM in terms of materials (organic and inorganic) to study osteogenesis in 3D. Therefore, this technique ensures the spatial distribution and cell loading efficiency, facilitates the detailed study of cell-biomaterial interactions, and results in the creation of highly structured and functional tissue constructs. This approach provides a bioprinted model to study osteogenesis and the early stages of tissue maturation *in vitro*. Therefore, the current work highlights the production of a tailored bioink and underlines its significant contribution to the development of a 3D model for studying the osteogenic differentiation of MSCs. The methodology presented in this study can be readily adapted for broader applications in personalized medicine, including 5D bioprinting. 5D bioprinting integrates 3D model construction with data on physiological activity, providing a powerful tool for personalized therapies, as demonstrated in previous studies [33,34]. Moreover, this alginate-based system holds potential for promising applications in toxicological testing using organoid models. This flexibility highlights the adaptability of our biofabrication approach, extending its utility to the broader contexts of 5D personalized medicine and organoid-based toxicological screening.

2. Results and Discussion

The aim of the study was to explore the combination of alginate, nHA and Col to create a composite ink for 3D bioprinting of constructs capable of replicating the composition of native bone ECM, facilitating *in vitro* studies on osteogenesis and contributing to reducing animal experimentation in the field of tissue engineering.

Alginate was used due to its properties, namely easy adjustability, low price, and accessibility [12,14,35]. Furthermore, the inclusion of nHA, a mineral, and Col, a protein, has been implemented due to their well-known capacity to enhance osteogenic potential and accelerate the regeneration of modular bone tissue [36]. Whilst the inclusion of hydroxyapatite in hydrogels can improve the osteogenic and rheological properties; Col can support high cell viability, proliferation and differentiation, providing an optimal microenvironment conducive to cell survival and functional performance of the printed composite [19,37,38].

The concentrations of alginate, nHA, and Col used in this study (2%, 0.5%, and 0.5%, respectively) were selected based on findings from previous research. A 2% alginate concentration was selected for its ideal balance of gel strength and printability, providing excellent gelling properties, structural integrity, and effective cell encapsulation and nutrient diffusion [39]. Additionally, the incorporation of 0.5% nHA and 0.5% Col is based on the research conducted by Hassani *et al.*, which demonstrated that these concentrations contribute to an osteogenic microenvironment favourable to the development of bone tissue. These concentration ratios were chosen to leverage their synergistic effects, aiming to enhance the osteogenic differentiation and the overall structural integrity of the hydrogel [27]. The selected concentrations are consistent with those used in similar studies, but preliminary experiments were conducted to test a range of concentrations for each component. The final concentrations achieved the best balance of printability, structural stability, and biological functionality, as verified by our data.

 doi:10.20944/preprints202410.1926.v1

The dual crosslinking methodology employed in this study follows a sequential process aimed at optimizing both the biological and mechanical properties of the hydrogel. Initially, Col fibrillogenesis was induced by raising the temperature to 37°C for 90 minutes, allowing the collagen component to self-assemble into fibrils that closely mimic the natural extracellular matrix. This step is key for promoting cell-matrix interactions, which support cellular adhesion and osteogenic differentiation. Afterwards, $CaCl_2$ solution was introduced to initiate the ionic crosslinking of alginate. Despite the rapid gelation of alginate upon contact with Ca^{2+} ions, the solution was left to interact for an extended period of 40 minutes. This duration was selected to ensure comprehensive crosslinking throughout the hydrogel matrix, thereby enhancing its mechanical stability and functional integrity. The sequential approach of collagen self-assembly followed by alginate crosslinking is essential for creating a composite hydrogel that balances bioactivity with mechanical strength [39]. The dual crosslinking methodology employed presents notable benefits, but it also has limitations, including potential spatial heterogeneity and extended processing times. Future research should aim to address these issues by improving the distribution of crosslinking agents, investigating more efficient methods, and optimizing cell encapsulation techniques to enhance the methodology's applicability and performance in tissue engineering [40–43].

3.1. Rheological Characterization

To achieve optimal print fidelity, several material properties, including viscoelastic behavior, must be considered to ensures that the bioink flows smoothly through the nozzle, maintaining high cell viability during deposition [44]. The viscoelastic characteristics of the crosslinked hydrogels were assessed through oscillatory rheology using amplitude and frequency sweep tests (Figure 1). First, the upper limit of the linear viscoelastic region (LVR) was determined from the storage modulus (G') curve assuming a ±5% deviation between two consecutive measurements at 0.1% oscillation strain (Figure 2a).

Amplitude sweep tests (Figure 1a) also demonstrated that both formulations exhibited a gel-like or solid structure behaviour in the LVR with a higher G' compared to the G'' (G'>G''). According to literature, viscoelastic solids present a higher storage modulus than loss modulus, due to the strong internal chemical bonds and physicochemical reactions in the material [45]. Considering constant amplitude and frequency conditions (1% strain, 1 Hz frequency), the G' was about ten times higher than the G'', indicating a solid elastic behavior for both formulations. Furthermore, the addition of nHA and Col did not appear to significantly alter LVR ($p>0.05$). Clearly from the results, nHA and Col did not seem to affect the initial characteristics of the hydrogel. The overall modulus of elasticity and loss values did not change between the gels.

Analysing Figure 1a also shows that the alginate-nHA-Col group presented a higher yield point (0.00974) compared to the alginate group (0.00864), suggesting that the addition of nHA and Col increased the material's resistance to initial deformation. Meanwhile, the flow point, indicating the transition to a viscous-dominated behavior, was lower in the alginate-nHA-Col group (0.0318) than in the alginate group (0.0685). This data suggest that although the composite hydrogel requires slightly more stress to begin yielding, it transitions to a flow state more readily, possibly due to the combination of the effects of the nHA reinforcement and the elastic behaviour of the Col. To further evaluate the transition from the LVR to the flow state, the flow transition index (ratio of flow point to yield point) was calculated. The alginate group presented a higher index (3.26) compared to the alginate-nHA-Col group (7.93), suggesting that the alginate-nHA-Col group is less tendency to brittle fracture [46].

Frequency sweeps were performed within the linear viscoelastic range (LVR) of both formulations at an oscillation strain of 0.1% (Figure 1b). The results demonstrated that both formulations exhibited viscoelastic gel-like properties, with no clear dependency of the G' or G" on frequency. Remarkably, a consistent difference of 8 kPa was observed between G' and G" across all tested frequencies for both formulations.

A non-dependence between these values and frequency suggests that the material's elastic and viscous properties were not influenced by the frequency of the applied stress. This is a characteristic

 doi:10.20944/preprints202410.1926.v1

of a gel that is stable and does not change its behavior significantly over a range of frequencies. This type of behavior is typical of gels that are well-formed, and it is often noted in materials that are used in applications where they need to maintain their structure and properties over time [47].

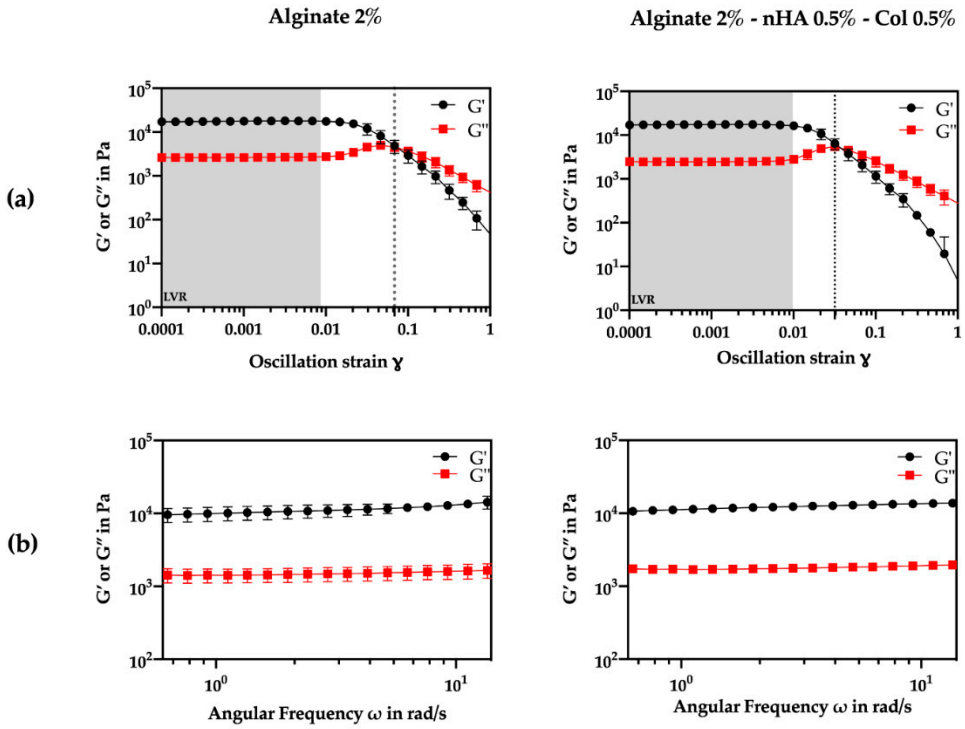

Figure 1. Rheological experiments with the storage moduli (G') (shown in black) and loss moduli (G'') (shown in red) of crosslinked alginate and alginate-nHA-Col under a range of conditions. (a) Amplitude sweeps performed at a frequency of 1 Hz. (b) Frequency sweeps perfromed at an oscillation strain of 0.1%. The evaluations were performed in triplicate.

3.2. *Mechanical Analysis*

The success of a hydrogel is highly dependent on its mechanical properties, as these properties ensure the hydrogel's structural integrity under both *in vitro* and *in vivo* conditions [48]. Parameters such as porosity, pore size, composition, degree of crosslinking, and ionic strength of materials can significantly influence their mechanical strength [49]. In the present work, the mechanical properties of alginate-based gels were evaluated through compressive mechanical testing. Figure 2 illustrates the compressive strength-strain curve and Table 1 provides the Young's modulus measurements of the alginate-based hydrogels.

Based on the stress-strain curve (Figure 2), the alginate-only hydrogel presented a lower stress-strain behavior due to its brittle nature, whereas the composite hydrogel comprising nHA and Col revealed higher stress-strain behavior due to the combined effects of nHA's reinforcement and Col's elasticity. nHA contributed to the reinforcement of the hydrogel matrix, distributing stress more evenly and enhancing the material's toughness and resistance to deformation [49]. On the other hand, Col, being a fibrous protein, provided elasticity and improved the tensile strength of the hydrogel, providing a more flexible matrix that could stretch further before rupturing [50]. The combination seemed to make the hydrogel more durable and capable of withstanding higher stresses and strains.

Young's modulus was calculated at 10% strain and the addition of 0.5% (w/v) nHA and 0.5% (w/v) of Col 0.5 wt % to alginate decreased Young's modulus of Alg hydrogel from 7.33 to 6.80 MPa (Table 1). Notwithstanding, no statistically significant differences were observed in the average Young's modulus between the two groups.

 doi:10.20944/preprints202410.1926.v1

Based on these findings, the hydrogel composed of only alginate appeared to have a higher initial stiffness (higher Young's modulus) but a lower capacity to withstand large deformations (lower stress-strain behaviour) due to its more fragile nature.

Meanwhile, the hydrogel composed of alginate, nHA and Col seemed to be more flexible initially (lower Young's modulus) and better able to withstand large deformations (higher stress-strain behaviour) due to the addition of Col, which increased elasticity, and nHA, which reinforced the matrix.

The combination of the different components in the hydrogel resulted in a material that can better absorb and dissipate stresses, resulting in greater deformation capacity and final strength, despite being initially more flexible.

The bioink formulation's rheological and mechanical properties were tailored to enhance the bioprinting process, allowing mimicry of the complex environment of the bone's ECM, which is crucial for supporting osteogenesis *in vitro*.

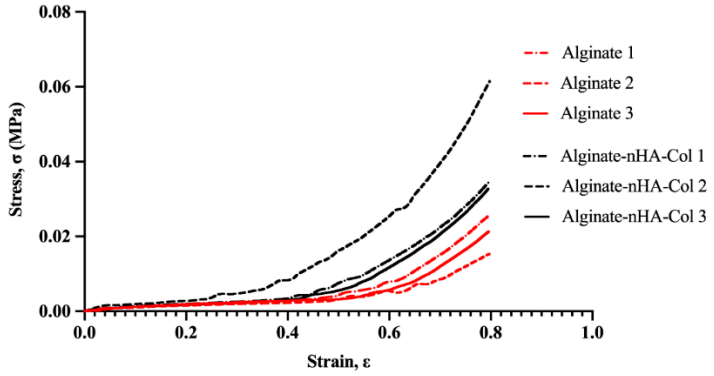

Figure 2. Stress–strain curves resulting from compression tests of alginate hydrogel (red) and alginate-nHA-Col hydrogel (black) (n=3).

Table 1. Young's modulus measurement of alginate and alginate-nHA-Col hydrogels produced (mean ± sd values) (n=3).

Parameter (MPa)	Alginate	Alginate-nHA-Col (w/v)	P value
Young's Modulus	7.33 ± 1.21	6.80 ± 0.835	0.567

3.3. Hydrogel Swelling Behaviour

The swelling properties play a fundamental role in facilitating the release of molecules, absorption of biofluids, and distribution of nutrients in the structure [36]. Swelling rates are an important feature of bioinks, with ideal formulations undergoing controlled degradation to facilitate new tissue growth [51–54]. Hydrogels intrinsically swell as solvent molecules infiltrate the spaces within the polymeric network. In 3D bioprinting, the extent of swelling is reflected in the dimensional alterations of bioprinted structures [55–57]. Moreover, the swelling ratio is essential in modulating the drug release dynamics from these polymeric systems [57–59]. Hydrogel swelling behavior (pH = 7.4 at 37°C) was evaluated at time intervals of 1, 2, 3, 4, 5, 24, 48 and 72 hours. The absorption of DPBS by the hydrogels is shown in Figure 3. The hydrogels appeared to absorb a significant amount of DPBS at first, and then more gradually over time. The hydrogel appeared to reach swelling equilibrium in a relatively short time (3 hours). The maximum swelling ratio was noted up to 24 hours. Then the swelling ratio significantly dropped in all the hydrogels due to the breakdown of the dry hydrogel system in the presence of DPBS.

Although the data were not significantly different, after 3 hours in culture, the hydrogel with nHA and Col seemed to increase the swelling compared to the hydrogel with alginate only. The incorporation of Col and nHA to alginate can increase the swelling rate of the resulting composite

 doi:10.20944/preprints202410.1926.v1

material due to the enhanced stability and mechanical strength of the alginate hydrogel, leading to a more controlled degradation rate. The incorporation of Col and nHA into alginate matrices may potentially influence the swelling rate of the resulting composite hydrogels. Col, being a hydrophilic material, presents more hydrophilic bonds, which can result in water retention and consequently affect the swelling behavior [60]. Additionally, the hydrophilic nature of hydroxyapatite in the material composition can lead to overall water absorption and potentially enhance cell growth, proliferation, and viability within the material [21]. For bone mimicry, a high degree of swelling is particularly important, as it allows cell infiltration into the hydrogels and maximizes cell growth within the structure [61].

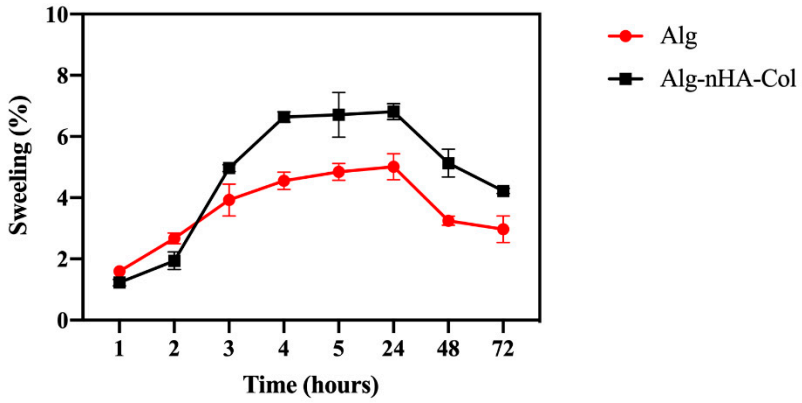

Figure 3. Hydrogel swelling rate from 1 to 72h. Alg: alginate (red); Alg-nHA-Col (black) (n=3).

3.4. Bioprinting of Cell-Laden Hydrogels

This study integrated bioprinting and pressure-assisted extrusion technologies in the printing protocols for alginate-based bionks. The printing process was carried out using the RegenHU 3D Discovery Evolution system with 2% (w/v) alginate bioinks. This formulation was selected based on prior studies due to its low viscosity and shear-thinning properties, making it suitable for bioprinting cellular inks[39]. The bioprinting parameters, including needle diameter, pressure, feed speed, filament distance, and thickness, were properly adjusted to establish an optimum equilibrium between printing resolution, speed, and cell activity (Table 2). The printing parameters were adjusted to guarantee high cell viability during the printing process whilst ensuring the extrusion of accurate filaments, with the external filament diameter corresponding the internal diameter of the nozzle used. This precision is of paramount importance to ensure the fidelity of the structural form in the final constructs, thus achieving an accurate physical replication of the digital CAD model (Figure 4A–C).

Given the low viscosity of the ink formulations used, without compromising shape fidelity [39], suspension bioprinting strategies were employed. A 0.5% (w/v) agarose support bath was utilized to maintain the structure of the printed material in suspension (Figure 4D). Once the material had been deposited and crosslinked, the suspension bath was removed and the hydrogels with the cells could grow.

 doi:10.20944/preprints202410.1926.v1

Table 2. Parameters used in the RegenHU 3D Discovery Evolution system. The values are shown in the respective units.

Parameters	Values (unit)
Needle Diameter	600 μm
Pressure	0.02 MPa
Feed Rate	10 mm/s
Filament Distance	500 mm
Thickness	500 mm

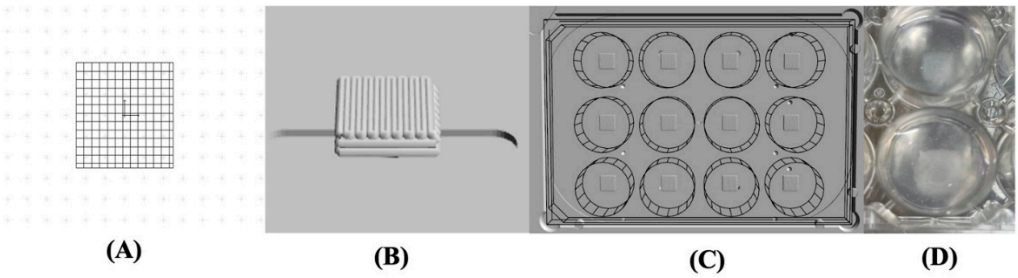

Figure 4. (A) CAD model designed in BioCAD™ software; (B) 3D generated model; (C) 3D generated model in a 12-well plate; (D) Cell-laden print in the agarose support bath.

3.5. Live/Dead Staining

Cell viability must be maintained both during and after the 3D tissue printing process. Therefore, an assessment of cell viability (hBMSCs) was performed using a Live/Dead analysis. This analysis was conducted after 1, 3, and 7 days in culture (Figure 5A,B).

The staining demonstrated high levels of cell viability in both alginate and alginate-nHA-Col hydrogels throughout all time points (Figure 5A).

The hBMSCs viability and distribution did not appear to depend on the inclusion of nHA and Col to the gel and the cells seemed to be homogeneously distributed in both hydrogels. In fact, some cell death was observed throughout the experiment, although this was to be expected due to exposure to significant shear stress during the printing process, which can cause cell damage and death [62]. Nevertheless, the results of the alginate-nHA-Col group indicated that live cell portions remained above 80% one week after processing (Figure 5B). It is important to note that alginate-nHA-Col group presented slightly higher values of cell viability, but with no significant differences when compared to the alginate group throughout the experiment.

In addition, data showed that a spherical cell morphology was preserved throughout the culture in both conditions. Maintaining a spherical cell morphology within bioinks is advantageous for preserving cell viability and functionality throughout the bioprinting process. This preservation of native cell structure is essential for ensuring proper differentiation into specific cell lineages, which is critical for effective tissue engineering applications [54].

These findings suggest that alginate-nHA-Col hydrogels were non-cytotoxic and provided a supportive matrix conducive to high cell viability of hBMSCs. The results confirmed the hydrogels' ability to sustain hBMSC culture, suggesting that the pressure-assisted extrusion process did not adversely affect cell viability.

 doi:10.20944/preprints202410.1926.v1

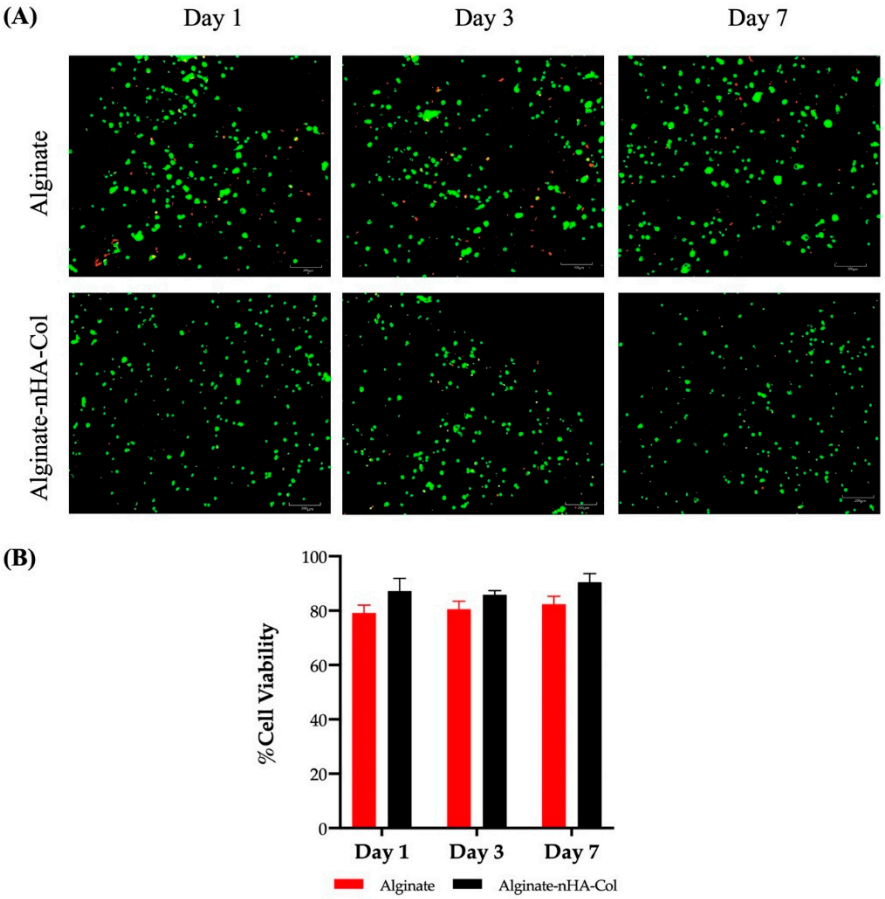

Figure 5. (A) Live/dead staining images of printed hBMSCs in alginate and alginate-nHA-Col after 1, 3 and 7 days in culture. Live cells are stained green and dead cells are stained red. (B) The percentage of cell viability of bioprinted hBMSCs cultured in 2% alginate and 2% alginate - 0.5% nHA - 0.5% Col for 1, 3 and 7 days (n=3).

3.6. Cell Viability Assay

In accordance with the ISO 10993-5:2009 guidelines, the assessment of cellular viability was determined using PrestoBlue™ on both alginate and alginate-nHA-Col hydrogels in the presence of hBMSCs. The control group, devoid of hydrogels was also included for reference. Figure 6A represents the corrected absorbance values for the designated time points (1, 3, 5, and 7 days). The data showed cell proliferation in all groups up to day 5. While the hydrogels containing alginate, nHA, and Col exhibited slightly higher cell viability rates compared to the other groups, statistically significant differences were only observed on day 3. In contrast, alginate-nHA-Col hydrogels showed significantly greater absorbance than the control group, suggesting enhanced cell adhesion and proliferation. These findings are consistent with previous studies, indicating that the alginate-nHA-Col hydrogels demonstrated superior cytocompatibility overall when compared to the control group [27].

Figure 6B displays the viability inhibition percentages, normalized to the control group. According to the ISO 10993-5:2009 guideline, a cytotoxic effect is considered when an inhibition of viability larger than 30% is identified (outlined in Figure 6B by dashed lines). These findings suggest that both alginate and alginate-nHA-Col can be classified as non-cytotoxic.

In agreement with the results presented in the Live/Dead analysis, the viability results confirmed that, on one hand, the hydrogels are supportive of hBMSCs encapsulation and function and, on the other, the printing process does not negatively impact on cell survival that remained viable for up to seven days post-encapsulation.

 doi:10.20944/preprints202410.1926.v1

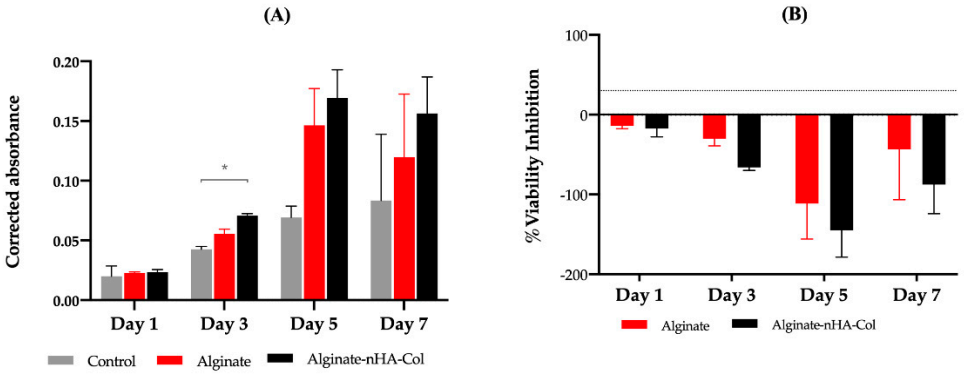

Figure 6. (A) Corrected absorbance evaluated by Presto Blue® viability assay for hBMSCs. Results significance are presented through the symbol (*), according to the P value, with *p<0.05. (B) % viability inhibition assay. The results were normalized in relation to the control. The 30% threshold shown (dashed line) represents the inhibition above which the effect is considered cytotoxic (under ISO 10993-5:2009 guidelines).

3.7. Gene Expression

Osteogenesis of hBMSCs cultured in alginate and alginate-nHA-Col for 7 and 14 days was evaluated using qPCR for a panel of key differentiation marker genes (Figure 7). This gene expression analysis provided insights into the biofunctionality and osteoinductive potential of the inks for bone tissue regeneration.

After 14 days of culture, gene expression analysis revealed a higher expression of osteogenic markers (Figure 7) in all experimental groups compared to the same groups after 7 days. At both time points, the expression of RUNX2 in the alginate-nHA-Col group was slightly higher than the alginate group at both time points (Figure 7A). RUNX2 is a gene expressed during early bone differentiation, and its increased expression from 7 to 14 days is consistent with expected osteogenic progression. Similarly, in the study by Im *et al.*, bioinks composed of alginate, tempo-oxidized cellulose nanofibrils, and polydopamine nanoparticles demonstrated an increase in RUNX2 gene expression over the same time period, further supporting these findings [8]. This gene plays a crucial role in regulating the osteogenic differentiation of hBMSCs and presence of this gene leads to the formation of mature osteoblasts and complete bone formation [63]. ALPL is associated with the biological process of endochondral ossification/ osteoblast differentiation [64] and showed a minimal increase from day 7 to day 14 (Figure 7B). Gene expression of IBSP demonstrated an increase in both groups from 7 to 14 days (Figure 7C). IBSP expression has been shown to increase the expression of key osteogenic and angiogenic markers, indicating its beneficial role in promoting the formation and vascularisation of bone tissue [65,66]. Furthermore, IBSP encodes bone sialoprotein, a protein involved in matrix production by promoting the nucleation of hydroxyapatite crystals during the mineralization process [67]. This trend was similarly observed in the study by Van der Heide *et al.*, where IBSP expression increased over time, confirming its role in bone mineralization [68].

Although not statistically significant, the expression of SPP1 in the alginate group was higher than in the alginate-nHA-Col group (Figure 7D). SPP1 is a crucial component of the organic matrix of bone and serves as a binding protein for osteoclasts, the cells responsible for bone remodeling [69].

COL1A2 was not expressed in any of the groups after 7 days (Figure 7E). However, after 14 days, the alginate-nHA-Col group showed an up-regulation of COL1A2 expression compared to the alginate group. The observed increase in COL1A2 gene expression aligns with findings reported in the literature [70]. Col is a major ECM protein synthesized by osteoblasts and significantly contributes to bone strength [71]. The observed increased expression of these osteoblastic genes in 3D hBMSCs constructs after 14 days suggests that the incorporation of alginate, nHA and Col elements in the bioink is important for enhancing osteogenic differentiation.

 doi:10.20944/preprints202410.1926.v1

The presence of bone-related gene expression in alginate-nHa-Col at day 14 also suggests a positive and sustained long-term osteogenic effect in hBMSCs. Nevertheless, osteogenic differentiation is a complex process that involves the sequential expression of several genetic markers at different times. For instance, early markers such as RUNX2 and osterix are expressed during the initial phases of differentiation, while later markers such as SPP1 and osteocalcin are associated with mature osteoblasts and mineralization [72]. As future research, it is important to evaluate genetic markers over an extended period, such as 21 days. In addition, further studies, such as staining with ALP and Alizarin Red, would be pertinent in providing better validation of the support's functionality and osteogenic differentiation.

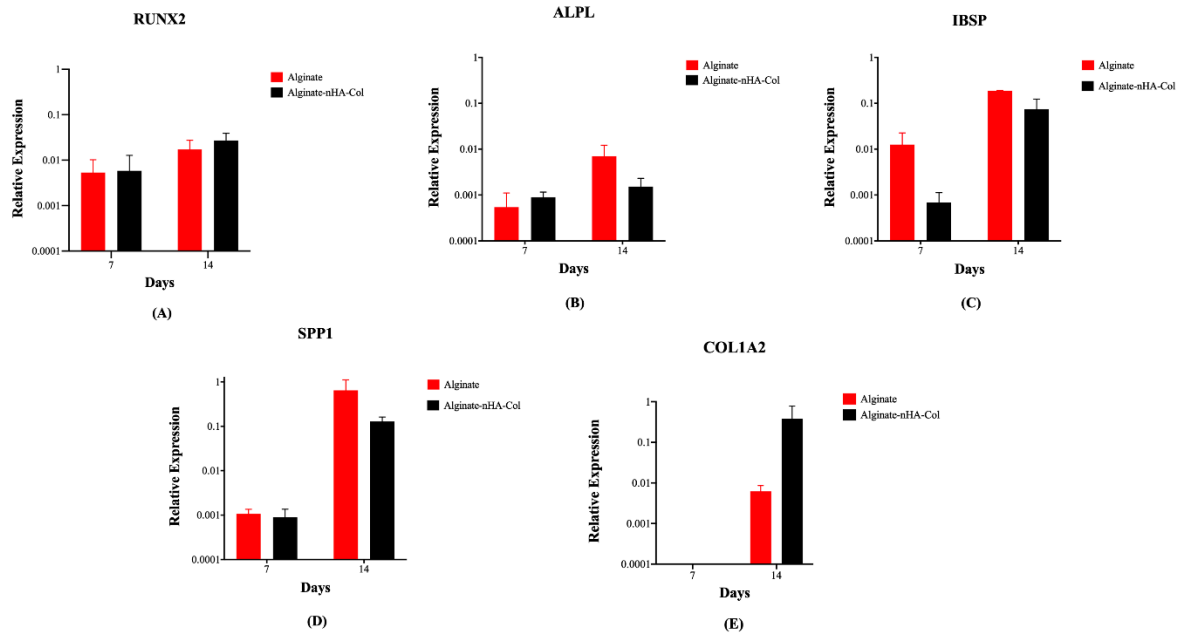

Figure 7. Gene expression levels of printed hBMSCs in alginate and alginate-nHA-Col bioinks following 7 and 14 days under osteogenic differentiation: runt-related transcription factor 2 (RUNX2) (A), alkaline phosphatase (ALPL) (B), integrin-binding sialoprotein (IBSP) (C), secreted phosphoprotein-1 (SPP1) (D) and collagen type 1 alpha 2 chain (COL1A2) (E).

3. Conclusions

The current work describes the successful development of a composite hydrogel bioink based on incorporated alginate, nHA, and Col, along with hBMSCs.

Rheological tests confirm that the viscoelastic properties are maintained with the addition of nHA and Col, while the mechanical tests showed that these additions enhance the hydrogel's performance under compressive stresses. LIVE/DEAD™ and PrestoBlue results confirm the ability of developed materials to support the encapsulation and printing of hBMSCs without significant loss cell viability 7 days post-printing. PCR analysis demonstrated that the alginate-nHA-col enhanced the expression of osteogenic markers in hBMSCs, suggesting the hydrogel's pro-osteogenic differentiation potential.

The incorporation of nHA and Col into alginate appears to have enhanced the physical and biological properties of the bioink, providing a promising 3D bioprinted model to mimic bone tissue. This study represents a significant step forward in the development of bioinks for this field, offering a viable and ethical solution for studying osteogenesis and early tissue maturation *in vitro*.

 doi:10.20944/preprints202410.1926.v1

4. Materials and Methods

4.1. Materials

Sodium alginate (#180947-100G), nHA (particle size < 200 nm; #677418-25G) and Col type I (#5074-35ML) were purchased from Sigma-Aldrich (Saint Louis, Missouri (MO), United States of America (USA)). The hydrogel formulations were prepared using an agarose (#A6013-100G) fluid gel bath also obtained from Sigma-Aldrich (Saint Louis, MO, USA). Subsequent to their production, the hydrogels were cross-linked using calcium chloride dihydrate ($CaCl_2.2H_2O$; #22317.230-250G), from VWR Chemicals (Pennsylvania, USA).

4.2. Preparation of Alginate-Based Solutions

The alginate solution was prepared by dissolving 4% (w/v) sodium alginate in Milli-Q water with continuous magnetic stirring overnight. Following this, the 4% alginate solution underwent sterilization via autoclaving and was subsequently subjected to a 1:1 dilution with Milli-Q water, resulting in the formulation of a 2% alginate solution. For the preparation of the alginate-nHA-Col solution, the 2% (w/v) alginate solution was combined with 0.5% (w/v) nHA and 0.5% (w/v) Col. Table 3 provides an overview of the compositions of the alginate-based solutions.

Table 3. Composition of alginate-based solutions.

Solutions	Sodium alginate (w/v)	nHA (w/v)	Col (w/v)
Alginate	2	-	-
Alginate-nHA-Col	2	0.5	0.5

4.3. Cell Culture and Maintenance

All experiments followed the relevant guidelines and were conducted with approvals from the NHS Health Research Authority National Research Ethics Service (21/NS/0056) and the University of Manchester, as well as written inform donor consent. The cells used in this study were previously isolated from bone marrow collected from a 49-year-old female donor after hip replacement surgery. The Strassburg *et al.* protocol was used to isolate the cells [73]. The hBMSCs were cultured under standard conditions in αMEM media (Sigma-Aldrich, # M4526) enriched with 10% (v/v) fetal bovine serum (FBS) (Gibco, #A3160802), 110 mg L^{-1} sodium pyruvate, 1000 mg L^{-1} glucose, 100 U mL^{-1} penicillin, 100 µg mL^{-1} streptomycin (Gibco, #15140122) and 0.25 µg mL^{-1} amphotericin (Gibco, #15290026) and 2 mM GlutaMAX (Gibco, #35050061). The hBMSCs were then maintained at 37°C in an 80% humidified atmosphere with 5% CO_2.

4.4. Oscillatory Rheological Measurements

The Anton Paar RheoCompass™ rheometer (MCR92, Anton Paar, Graz, Austria) operated with Anton Paar RheoCompass v1.30.1164 software was used to evaluate the rheological properties of the samples. Measurements were conducted using a PP12.5 measuring plate, featuring a diameter of 12.5 mm and a 1 mm gap. Alginate-based hydrogels with different compositions (as detailed in Table 4) were prepared following the transwell methodology. Briefly, 400 µL of the solution was pipetted onto 12-well plate transwell inserts. The alginate-nHA-Col hydrogels gelation was achieved through a dual-crosslinking procedure. Initially, Col crosslinking was induced by incubating at 37°C for 90 minutes. Subsequently, the alginate was gelled using 150 µM calcium chloride ($CaCl_2$) solution in Milli-Q water for 40 minutes, as the process used for alginate-only hydrogels. Finally, the hydrogels were removed from the inserts and washed with DPBS.

The measurement conditions were as follows: Amplitude Sweep: Temperature =25°C, Frequency = 1 Hz, Oscillation Strain = 0.01–100%; Frequency Sweep: Temperature =25°C, Frequency = 0.1 - 10 Hz, Oscillation Strain = 0.1%. The data was measured in triplicate and the results were shown as mean ± standard deviation.

 doi:10.20944/preprints202410.1926.v1

4.5. Hydrogel Swelling Behavior

Hydrogel swelling behavior was assessed under physiological conditions (pH = 7.4 at 37°C). Initially, the weight of the hydrogels (prepared as outlined in section 4.3) was measured post-crosslinking using precision scales (GR-300-EC, A&D Instruments, United Kingdom). Subsequently, these hydrogels were immersed in DPBS at 37°C within a 12-well plate, and the weight of the swollen hydrogels was recorded. At specific time intervals (1, 2, 3, 4, 24, 48, and 72 hours), the hydrogels were reweighed after blotting off excess water with tissue paper. The swelling behavior was quantified as a percentage of the swelling ratio, computed using Equation I.

$$\text{Swelling ratio (\%)} = (Wf - Wi)/Wi \times 100, \quad \text{(I)}$$

Wf and Wi are final and initial weight of the hydrogel (in g), respectively.

4.6. Mechanical Analysis

Compressive strength and Young's modulus (expressed in kPa) of the hydrogels were assessed using the ElectroForce 5500® Test instrument (TA Instruments, Delaware, USA) equipped with a 5 N load cell. Alginate and alginate-nHA-Col hydrogels (prepared as outlined in section 2.2 of the Materials and Methods) were tested in triplicate, each sample having a height of 3 mm and a diameter of 12 mm. A compression test was conducted employing a flat probe with a diameter of 10 mm and a cross-head displacement rate of 2.0 mm/min. Compression was continued until 80% strain was reached. The compressive (Young's) modulus was determined by calculating the slope of the linear portion of the stress-strain curve at 10% strain. The settings for the loading procedure were programmed using the WinTest® Software (TA instruments). The real-time monitoring of the applied load was performed using the WinTest® Software.

4.7. Bioprinting of Cell-Laden Hydrogels

A pressure-assisted extrusion printer (3D Discovery, RegenHU, Villaz-St-Pierre, Switzerland) with an enclosed biosafety cabinet was employed in the fabrication of cell-laden constructs (Figure 8A). Alginate-based inks loaded with hBMSCs at a density of 2 x 10^6 cells/mL were prepared as described in the section 2.2 and 2.3 and printed inside a suspension bath of agarose particles (Figure 8B) [74], using a set of process parameters previously optimized in our lab. The suspension bath was prepared based on a protocol originally reported by Moxon *et al.* [75].

Square-based scaffolds (6 x 6 mm) were designed using BioCAM™ software (RegenHU, Villaz-St-Pierre, Switzerland) and printed in 12-well plates under sterile conditions and at room temperature. Following bioprinting, crosslinking was performed in a two-step process. Initially, Col fibrils were allowed to self-assemble for 90 minutes at 37°C. Subsequently, a $CaCl_2$ solution was added to the wells and incubated for 40 minutes at 37°C to induce the crosslinking of alginate. The cell-laden hydrogels were then rinsed with DPBS and cultured in αMEM medium at 37°C under 5% CO_2 and 80% humidity.

 doi:10.20944/preprints202410.1926.v1

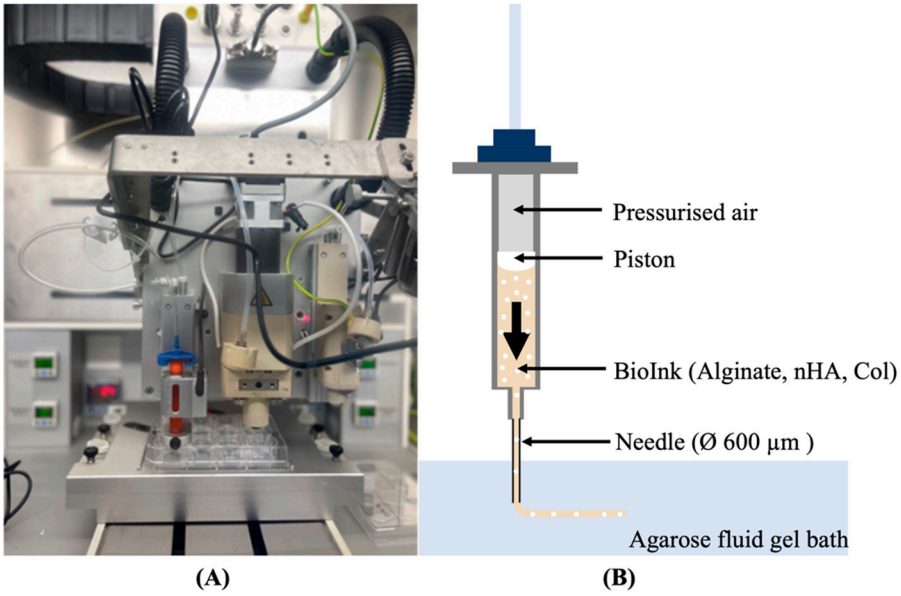

Figure 8. (A) 3D Discovery Evolution bioprinter; (B) Schematic representation of the pressure-assisted extrusion process, in which pressurized air drives the bioink from the bioprinter cartridge through a needle into a well plate containing a suspension bath.

4.8. Live/Dead Staining

A Live/Dead assay kit (Invitrogen™ #L3224) was used to evaluate the viability of hBMSCs cultured on alginate and alginate-nHA-Col hydrogels. According to the manufacturer's protocol, 600 µL of assay solution containing 4 µM ethidium homodimer-1 (EthD-1) and 2 µM calcein AM was added to the cell-hydrogel constructs. After a 20-minute incubation, the cells were washed with DPBS and imaged using the CellVoyager™ CQ1 Benchtop High-Content Analysis System (Yokogawa, Japan) with an excitation wavelength of 495 nm. Cell imaging was conducted at one, three, and seven days post-culture, with three images acquired per time point. The acquired images were systematically analysed and subsequently the number of cells quantified using ImageJ2 software (version: 2.3.0/1.53q). Cell viability was assessed by calculating the ratio of live cells to the total cell count. To ensure reproducibility, all measurements were conducted in triplicate at each time point.

4.9. Cell Viability Assay

To evaluate the cellular viability of hBMSCs within alginate-based hydrogels, the PrestoBlue™ (InvitrogenTM #A13261) assay was performed at one, three, five, and seven days. The evaluation was performed as previously described [21]. In brief, at each timepoint, the culture media was aspirated and substituted with fresh complete media supplemented with 10% (v/v) of the PrestoBlueTM reagent.

After a one-hour incubation at 37°C in a controlled environment with 80% humidity and 5% CO_2, the supernatant media were transferred to a 96-well plate. Absorbance measurements were taken at 570 nm and 595 nm using a SPARK® multimode microplate reader (TECAN, Männedorf, Switzerland). Cell viability was quantified through absorbance spectroscopy by calculating the corrected absorbance, determined by subtracting the absorbance at 595 nm (used for normalization) from that at 570 nm (reflecting the experimental outcome). The resulting values were further adjusted by subtracting the average absorbance of control wells from that of the experimental wells. Residual substances were removed by gently washing the cells with DPBS, and fresh culture medium was added to each well.

 doi:10.20944/preprints202410.1926.v1

4.10. Gene Expression

To quantify gene expression levels, RNA extraction and complementary DNA (cDNA) synthesis were performed following established protocols [76,77]. Quantitative real-time polymerase chain reaction (qPCR) were carried out on a StepOnePlus system (Applied Biosystems), utilizing pre-designed intron-spanning primers (Sigma Aldrich) (Table 4). In brief, a total of 10 ng cDNA was added to each reaction in addition to 5µl of Fast SYBR Green Reagent, 1µl of forward primer, 1µl of reverse primer, and 2.5µl of molecular biology grade water.

cDNA synthesized in-house from Total Human RNA (Clontech) served as the positive control in this study. The levels of osteogenic genes were standardized by normalization against the pre-validated reference gene GAPDH [78].

Table 4. Name, accession number, forward/ reverse sequences, and concentrations of the primers used to assess osteogenic differentation.

Primer	Accession Number	Forward Primer Sequence 5′-3′	Reverse Primer Sequence 5′-3′	Concentration (nM)
glyceraldehyde-3-phosphate dehydrogenase (GAPDH)	NM_001256799	CTCCTCTGACTTCAACAG	CGTTGTCATACCAGGAAA	600
runt-related transcription factor 2 (RUNX2)	NM_001024630	CGCTGCAACAAGACC	CGCCATGACAGTAACC	900
alkaline phosphatase (ALPL)	NM_000478	ACGTCTTCACATTTGGTG	GGTAGTTGTTGTGAGCATA	450
integrin-binding sialoprotein (IBSP)	NM_004967	GACTGCTTTAATTTTGCTCAG	GTCACTACTGCCCTGAAC	600
secreted phosphoprotein-1 (SPP1)	NM_001040058	CTGACATCCAGTACCCTG	CAGCTGACTCGTTTCATA	600
collagen type 1 alpha 2 chain (COL1A2)	NM_000089	TGAAGCTGGTCCCCAAGGA	AATACCAGGAGCGCGCCGTTG	300

4.11. Statistical Analysis

To ensure experimental reproducibility, all experiments were performed in biological triplicates to capture variability between samples, and each assay was conducted in technical triplicates to account for within-experiment variability.

Statistical tests were carried out using GraphPad Prism® (version 10.3.1 for mac OS, La Jolla, California (CA), USA). Results were presented as mean ± standard error of the mean (SE). Comparisons between groups were made using one-way ANOVA, followed by Tukey's multiple comparisons test. Exclusively for the comparison of gene expression, a Mann-Whitney-U test was used. Statistical significance was acknowledged solely when $p \leq 0.05$. Significance levels were denoted by asterisks (*), with *p<0.05, **p<0.01, ***p<0.001 and ****p<0.0001.

Author Contributions: Conceptualization, A.C.S., M.D. and A.C.M.; methodology, A.C.S., G.M. and F.S.; validation, A.C.S., G.M. and F.S.; formal analysis, A.C.S., G.M., F.S. and M.D.; investigation, A.C.S., G.M., F.S., R.A., B.L., P.S., A.M. and A.C.; resources, J.D.S., L.A., N.A., S.R., M.D. and A.C.M..; data curation, A.C.S., G.M. and F.S.; writing—original draft preparation, A.C.S.; writing—review and editing, R.A., J.D.S., L.A., N.A., and A.C.M.; visualization, A.C.S., G.M., F.S., R.A., B.L., P.S., A.M., A.C., J.D.S., L.A., N.A., S.R., M.D. and A.C.M.; supervision, J.D.S., L.A., N.A., S.R., M.D. and A.C.M.; project administration, M.D. and A.C.M; funding acquisition, S.R., M.D. and A.C.M. All authors have read and agreed to the published version of the manuscript.

Funding: Ana Catarina Sousa (SFRH/BD/146689/2019), Bruna Lopes (2021.05265.BD), Patrícia Sousa (2023.00246.BD), André Coelho (2023.00428.BD), Alícia Moreira (2023.00544.BD) and acknowledge Fundação para a Ciência e Tecnologia (FCT), for financial support. Rui Alvites acknowledges the CECA, UP, and FCT for the funding and accessibility of all technical, structural, and human resources necessary for the development of this work. The work was supported through the project UIDB/00211/2020 funded by FCT/MCTES, national funds. This research was funded by Projects PEst-OE/AGR/UI0211/2011 from FCT, and COMPETE 2020, from ANI–Projetos ID&T Empresas em Copromoção, by the project "InnovaBIOMAS - Optimized Additive Biofabrication System for the Production of Hierarchical Multi-Tissue Scaffolds Applied in the Treatment of Joint Diseases" with the reference 2022.10564.PTDC, by the project "Bone2Move- Development of "in vivo"

 doi:10.20944/preprints202410.1926.v1

experimental techniques and modelling methodologies for the evaluation of 4D scaffolds for bone defect in sheep model: an integrative research approach" with the reference POCI-01-0145-FEDER-031146. Marco Domingos would like to thank the Henry Royce Institute EPSRC grants EP/R00661X/1, EP/S019367/1, EP/P025021/1 and EP/P025498/1.

Institutional Review Board Statement: Not applicable.

Informed Consent Statement: The study was conducted in accordance with the Declaration of Helsinki and approved by the NHS Health Research Authority National Research Ethics Service (number: 21/NS/0056) and the University of Manchester.

Data Availability Statement: Not applicable.

Acknowledgments: Not applicable.

Conflicts of Interest: The authors declare no conflicts of interest.

List of Abbreviations

3D	three-dimensional
ALPL	alkaline phosphatase
$CaCl_2$	calcium chloride
Col	collagen
COL1A2	collagen type 1 alpha 2 chain
DPBS	dulbecco's phosphate-buffered saline
ECM	extracellular matrix
FBS	fetal bovine serum
G′	storage modulus
G′′	loss modulus
IBSP	integrin-binding sialoprotein
hBMSC	human bone marrow stem/stromal cell
HA	hydroxyapatite
LVR	linear viscoelastic region
MSC	mesenchymal stem/stromal cell
nHA	nano-hydroxyapatite
qPCR	quantitative real-time polymerase chain reaction
RUNX2	runt-related transcription factor 2
SPP1	secreted phosphoprotein-1
SE	standard deviation of the mean

References

1. Wu, A.-M.; Bisignano, C.; James, S.L.; Abady, G.G.; Abedi, A.; Abu-Gharbieh, E.; Alhassan, R.K.; Alipour, V.; Arabloo, J.; Asaad, M.; et al. Global, regional, and national burden of bone fractures in 204 countries and territories, 1990–2019: a systematic analysis from the Global Burden of Disease Study 2019. *The Lancet Healthy Longevity* **2021**, *2*, e580-e592, doi:10.1016/S2666-7568(21)00172-0.
2. Polinder, S.; Haagsma, J.; Panneman, M.; Scholten, A.; Brugmans, M.; Van Beeck, E. The economic burden of injury: Health care and productivity costs of injuries in the Netherlands. *Accid Anal Prev* **2016**, *93*, 92-100, doi:10.1016/j.aap.2016.04.003.
3. Borgström, F.; Karlsson, L.; Ortsäter, G.; Norton, N.; Halbout, P.; Cooper, C.; Lorentzon, M.; McCloskey, E.V.; Harvey, N.C.; Javaid, M.K.; et al. Fragility fractures in Europe: burden, management and opportunities. *Arch Osteoporos* **2020**, *15*, 59, doi:10.1007/s11657-020-0706-y.
4. Caddeo, S.; Boffito, M.; Sartori, S. Tissue Engineering Approaches in the Design of Healthy and Pathological In Vitro Tissue Models. *Front Bioeng Biotechnol* **2017**, *5*, 40, doi:10.3389/fbioe.2017.00040.
5. Owen, R.; Reilly, G.C. In vitro Models of Bone Remodelling and Associated Disorders. *Frontiers in Bioengineering and Biotechnology* **2018**, *6*, doi:10.3389/fbioe.2018.00134.
6. Kwakwa, K.A.; Vanderburgh, J.P.; Guelcher, S.A.; Sterling, J.A. Engineering 3D Models of Tumors and Bone to Understand Tumor-Induced Bone Disease and Improve Treatments. *Curr Osteoporos Rep* **2017**, *15*, 247-254, doi:10.1007/s11914-017-0385-9.
7. Tripathi, S.; Mandal, S.S.; Bauri, S.; Maiti, P. 3D bioprinting and its innovative approach for biomedical applications. *MedComm (2020)* **2023**, *4*, e194, doi:10.1002/mco2.194.

8. Im, S.; Choe, G.; Seok, J.M.; Yeo, S.J.; Lee, J.H.; Kim, W.D.; Lee, J.Y.; Park, S.A. An osteogenic bioink composed of alginate, cellulose nanofibrils, and polydopamine nanoparticles for 3D bioprinting and bone tissue engineering. *International Journal of Biological Macromolecules* **2022**, *205*, 520-529, doi:https://doi.org/10.1016/j.ijbiomac.2022.02.012.
9. Vanderburgh, J.P.; Guelcher, S.A.; Sterling, J.A. 3D bone models to study the complex physical and cellular interactions between tumor and the bone microenvironment. *J Cell Biochem* **2018**, *119*, 5053-5059, doi:10.1002/jcb.26774.
10. Gonzalez-Fernandez, T.; Sikorski, P.; Leach, J.K. Bio-instructive materials for musculoskeletal regeneration. *Acta Biomater* **2019**, *96*, 20-34, doi:10.1016/j.actbio.2019.07.014.
11. Gonzalez-Fernandez, T.; Tenorio, A.J.; Campbell, K.T.; Silva, E.A.; Leach, J.K. Alginate-Based Bioinks for 3D Bioprinting and Fabrication of Anatomically Accurate Bone Grafts. *Tissue Eng Part A* **2021**, *27*, 1168-1181, doi:10.1089/ten.TEA.2020.0305.
12. Datta, S. Advantage of Alginate Bioinks in Biofabrication for Various Tissue Engineering Applications. *International Journal of Polymer Science* **2023**, *2023*, 6661452, doi:https://doi.org/10.1155/2023/6661452.
13. Mahmud, R.U.; Rahman, M.Z. 13.13 - Synthesis and characterization of nanocomposites for tissue engineering. In *Comprehensive Materials Processing (Second Edition)*, Hashmi, S., Ed.; Elsevier: Oxford, 2024; pp. 241-269.
14. Hariyadi, D.M.; Islam, N. Current Status of Alginate in Drug Delivery. *Advances in Pharmacological and Pharmaceutical Sciences* **2020**, *2020*, 8886095, doi:https://doi.org/10.1155/2020/8886095.
15. Shams, E.; Barzad, M.S.; Mohamadnia, S.; Tavakoli, O.; Mehrdadfar, A. A review on alginate-based bioinks, combination with other natural biomaterials and characteristics. *Journal of Biomaterials Applications* **2022**, *37*, 355-372, doi:10.1177/08853282221085690.
16. Sudipto, D.; Ranjit, B.; Jonali, D. Importance of Alginate Bioink for 3D Bioprinting in Tissue Engineering and Regenerative Medicine. In *Alginates*, Leonel, P., Ed.; IntechOpen: Rijeka, 2019; p. Ch. 7.
17. Ma, C.; Du, T.; Niu, X.; Fan, Y. Biomechanics and mechanobiology of the bone matrix. *Bone Research* **2022**, *10*, 59, doi:10.1038/s41413-022-00223-y.
18. Bielajew, B.J.; Hu, J.C.; Athanasiou, K.A. Collagen: quantification, biomechanics and role of minor subtypes in cartilage. *Nature Reviews Materials* **2020**, *5*, 730-747, doi:10.1038/s41578-020-0213-1.
19. Li, Z.; Ruan, C.; Niu, X. Collagen-based bioinks for regenerative medicine: Fabrication, application and prospective. *Medicine in Novel Technology and Devices* **2023**, *17*, 100211, doi:https://doi.org/10.1016/j.medntd.2023.100211.
20. Li, Y.; Liu, Y.; Li, R.; Bai, H.; Zhu, Z.; Zhu, L.; Zhu, C.; Che, Z.; Liu, H.; Wang, J.; et al. Collagen-based biomaterials for bone tissue engineering. *Materials & Design* **2021**, *210*, 110049, doi:https://doi.org/10.1016/j.matdes.2021.110049.
21. Sousa, A.C.; Biscaia, S.; Alvites, R.; Branquinho, M.; Lopes, B.; Sousa, P.; Valente, J.; Franco, M.; Santos, J.D.; Mendonça, C.; et al. Assessment of 3D-Printed Polycaprolactone, Hydroxyapatite Nanoparticles and Diacrylate Poly(ethylene glycol) Scaffolds for Bone Regeneration. *Pharmaceutics* **2022**, *14*, doi:10.3390/pharmaceutics14122643.
22. Sancilio, S.; Gallorini, M.; Di Nisio, C.; Marsich, E.; Di Pietro, R.; Schweikl, H.; Cataldi, A. Alginate/Hydroxyapatite-Based Nanocomposite Scaffolds for Bone Tissue Engineering Improve Dental Pulp Biomineralization and Differentiation. *Stem Cells Int* **2018**, *2018*, 9643721, doi:10.1155/2018/9643721.
23. Quinlan, E.; López-Noriega, A.; Thompson, E.; Kelly, H.M.; Cryan, S.A.; O'Brien, F.J. Development of collagen-hydroxyapatite scaffolds incorporating PLGA and alginate microparticles for the controlled delivery of rhBMP-2 for bone tissue engineering. *J Control Release* **2015**, *198*, 71-79, doi:10.1016/j.jconrel.2014.11.021.
24. Soleymani, S.; Naghib, S.M. 3D and 4D printing hydroxyapatite-based scaffolds for bone tissue engineering and regeneration. *Heliyon* **2023**, *9*, e19363, doi:https://doi.org/10.1016/j.heliyon.2023.e19363.
25. Melo, P.; Montalbano, G.; Fiorilli, S.; Vitale-Brovarone, C. 3D Printing in Alginic Acid Bath of In-Situ Crosslinked Collagen Composite Scaffolds. *Materials (Basel)* **2021**, *14*, doi:10.3390/ma14216720.
26. Chen, Y.; Zhou, Y.; Wang, C. Investigation of Collagen-Incorporated Sodium Alginate Bioprinting Hydrogel for Tissue Engineering. *Journal of Composites Science* **2022**, *6*, 227.
27. Hassani, A.; Khoshfetrat, A.B.; Rahbarghazi, R.; Sakai, S. Collagen and nano-hydroxyapatite interactions in alginate-based microcapsule provide an appropriate osteogenic microenvironment for modular bone tissue formation. *Carbohydrate Polymers* **2022**, *277*, 118807, doi:https://doi.org/10.1016/j.carbpol.2021.118807.
28. Campos, J.M.; Sousa, A.C.; Caseiro, A.R.; Pedrosa, S.S.; Pinto, P.O.; Branquinho, M.V.; Amorim, I.; Santos, J.D.; Pereira, T.; Mendonça, C.M.; et al. Dental pulp stem cells and Bonelike(®) for bone regeneration in ovine model. *Regen Biomater* **2019**, *6*, 49-59, doi:10.1093/rb/rby025.
29. Merimi, M.; El Majzoub, R.; Lagneaux, L.; Agha, D.; Fatima, B.; Meuleman, N.; Fahmi, H.; Lewalle, P.; Mohammad, F.-K.; Najar, M. The Therapeutic Potential of Mesenchymal Stromal Cells for Regenerative Medicine: Current Knowledge and Future Understandings. *Frontiers in Cell and Developmental Biology* **2021**, *9*, doi:10.3389/fcell.2021.661532.

30. Aleynik, D.; Charykova, I.; Rubtsova, Y.; Linkova, D.; Farafontova, E.; Egorikhina, M. Specific Features of the Functional Activity of Human Adipose Stromal Cells in the Structure of a Partial Skin-Equivalent. *International Journal of Molecular Sciences* **2024**, *25*, 6290, doi:10.3390/ijms25126290.
31. Sai, B.; Dai, Y.; Fan, S.; Wang, F.; Wang, L.; Li, Z.; Tang, J.; Wang, L.; Zhang, X.; Zheng, L.; et al. Cancer-educated mesenchymal stem cells promote the survival of cancer cells at primary and distant metastatic sites via the expansion of bone marrow-derived-PMN-MDSCs. *Cell Death & Disease* **2019**, *10*, 941, doi:10.1038/s41419-019-2149-1.
32. Kemp, K.C.; Hows, J.; Donaldson, C. Bone marrow-derived mesenchymal stem cells. *Leuk Lymphoma* **2005**, *46*, 1531-1544, doi:10.1080/10428190500215076.
33. Foresti, R.; Rossi, S.; Pinelli, S.; Alinovi, R.; Sciancalepore, C.; Delmonte, N.; Selleri, S.; Caffarra, C.; Raposio, E.; Macaluso, G.; et al. In-vivo vascular application via ultra-fast bioprinting for future 5D personalised nanomedicine. *Scientific Reports* **2020**, *10*, 3205, doi:10.1038/s41598-020-60196-y.
34. Lai, J.; Wang, M. Developments of additive manufacturing and 5D printing in tissue engineering. *Journal of Materials Research* **2023**, *38*, 4692-4725.
35. Datta, S. Advantage of alginate bioinks in biofabrication for various tissue engineering applications. *International Journal of Polymer Science* **2023**, *2023*.
36. Hassani, A.; Avci, Ç.B.; Kerdar, S.N.; Amini, H.; Amini, M.; Ahmadi, M.; Sakai, S.; Bagca, B.G.; Ozates, N.P.; Rahbarghazi, R.; et al. Interaction of alginate with nano-hydroxyapatite-collagen using strontium provides suitable osteogenic platform. *Journal of Nanobiotechnology* **2022**, *20*, 310, doi:10.1186/s12951-022-01511-9.
37. Ojeda, E.; García-Barrientos, Á.; Martínez de Cestafe, N.; Alonso, J.M.; Pérez-González, R.; Sáez-Martínez, V. Nanometric Hydroxyapatite Particles as Active Ingredient for Bioinks: A Review. *Macromol* **2022**, *2*, 20-29, doi:10.3390/macromol2010002.
38. Li, N.; Guo, R.; Zhang, Z.J. Bioink Formulations for Bone Tissue Regeneration. *Front Bioeng Biotechnol* **2021**, *9*, 630488, doi:10.3389/fbioe.2021.630488.
39. Ferreira, M.J.S.L.M. Integrating 3D Bioprinting and Pluripotent Stem Cell Technologies for Articular Cartilage Tissue Engineering. The University of Manchester, 2022.
40. Chen, Z.-Y.; Gao, S.; Zhou, R.-B.; Wang, R.-D.; Zhou, F. Dual-crosslinked networks of superior stretchability and toughness polyacrylamide-carboxymethylcellulose hydrogel for delivery of alendronate. *Materials & Design* **2022**, *217*, 110627, doi:https://doi.org/10.1016/j.matdes.2022.110627.
41. Kajave, N.S.; Schmitt, T.; Nguyen, T.U.; Kishore, V. Dual crosslinking strategy to generate mechanically viable cell-laden printable constructs using methacrylated collagen bioinks. *Mater Sci Eng C Mater Biol Appl* **2020**, *107*, 110290, doi:10.1016/j.msec.2019.110290.
42. Shehzad, A.; Mukasheva, F.; Moazzam, M.; Sultanova, D.; Abdikhan, B.; Trifonov, A.; Akilbekova, D. Dual-Crosslinking of Gelatin-Based Hydrogels: Promising Compositions for a 3D Printed Organotypic Bone Model. *Bioengineering* **2023**, *10*, 704.
43. Naranjo-Alcazar, R.; Bendix, S.; Groth, T.; Gallego Ferrer, G. Research Progress in Enzymatically Cross-Linked Hydrogels as Injectable Systems for Bioprinting and Tissue Engineering. *Gels* **2023**, *9*, 230, doi:10.3390/gels9030230.
44. Bercea, M. Rheology as a Tool for Fine-Tuning the Properties of Printable Bioinspired Gels. *Molecules* **2023**, *28*, doi:10.3390/molecules28062766.
45. Kostenko, A.; Connon, C.J.; Swioklo, S. Storable Cell-Laden Alginate Based Bioinks for 3D Biofabrication. *Bioengineering (Basel)* **2022**, *10*, doi:10.3390/bioengineering10010023.
46. Paar, A. Amplitude sweeps. Available online: https://wiki.anton-paar.com/uk-en/amplitude-sweeps/#:~:text=The%20limit%20of%20the%20linear,with%20the%20lowest%20strain%20values. (accessed on 31-12-2024).
47. Kocen, R.; Gasik, M.; Gantar, A.; Novak, S. Viscoelastic behaviour of hydrogel-based composites for tissue engineering under mechanical load. *Biomedical Materials* **2017**, *12*, 025004, doi:10.1088/1748-605X/aa5b00.
48. Shaabani, A.; Sedghi, R.; Motasadizadeh, H.; Dinarvand, R. Self-healable conductive polyurethane with the body temperature-responsive shape memory for bone tissue engineering. *Chemical Engineering Journal* **2021**, *411*, 128449, doi:https://doi.org/10.1016/j.cej.2021.128449.
49. Martinez, A.W.; Caves, J.M.; Ravi, S.; Li, W.; Chaikof, E.L. Effects of crosslinking on the mechanical properties, drug release and cytocompatibility of protein polymers. *Acta Biomaterialia* **2014**, *10*, 26-33, doi:https://doi.org/10.1016/j.actbio.2013.08.029.
50. Yi, B.; Xu, Q.; Liu, W. An overview of substrate stiffness guided cellular response and its applications in tissue regeneration. *Bioact Mater* **2022**, *15*, 82-102, doi:10.1016/j.bioactmat.2021.12.005.
51. Sharma, R.; Kirsch, R.; Valente, K.P.; Perez, M.R.; Willerth, S.M. Physical and Mechanical Characterization of Fibrin-Based Bioprinted Constructs Containing Drug-Releasing Microspheres for Neural Tissue Engineering Applications. *Processes* **2021**, *9*, doi:10.3390/pr9071205.
52. Moeinzadeh, S.; Jabbari, E. Gelation characteristics, physico-mechanical properties and degradation kinetics of micellar hydrogels. *Eur Polym J* **2015**, *72*, 566-576, doi:10.1016/j.eurpolymj.2015.04.028.

53. Rizwan, M.; Chan, S.W.; Comeau, P.A.; Willett, T.L.; Yim, E.K.F. Effect of sterilization treatment on mechanical properties, biodegradation, bioactivity and printability of GelMA hydrogels. *Biomedical Materials* **2020**, *15*, 065017, doi:10.1088/1748-605X/aba40c.
54. Wu, Z.; Su, X.; Xu, Y.; Kong, B.; Sun, W.; Mi, S. Bioprinting three-dimensional cell-laden tissue constructs with controllable degradation. *Scientific Reports* **2016**, *6*, 24474, doi:10.1038/srep24474.
55. Wei, L.; Li, Z.; Li, J.; Zhang, Y.; Yao, B.; Liu, Y.; Song, W.; Fu, X.; Wu, X.; Huang, S. An approach for mechanical property optimization of cell-laden alginate-gelatin composite bioink with bioactive glass nanoparticles. *J Mater Sci Mater Med* **2020**, *31*, 103, doi:10.1007/s10856-020-06440-3.
56. Mao, Q.; Wang, Y.; Li, Y.; Juengpanich, S.; Li, W.; Chen, M.; Yin, J.; Fu, J.; Cai, X. Fabrication of liver microtissue with liver decellularized extracellular matrix (dECM) bioink by digital light processing (DLP) bioprinting. *Materials Science and Engineering: C* **2020**, *109*, 110625.
57. Liu, W.; Borrell, M.A.; Venerus, D.C.; Mieler, W.F.; Kang-Mieler, J.J. Characterization of biodegradable microsphere-hydrogel ocular drug delivery system for controlled and extended release of ranibizumab. *Translational vision science & technology* **2019**, *8*, 12-12.
58. Li, Z.; Huang, S.; Liu, Y.; Yao, B.; Hu, T.; Shi, H.; Xie, J.; Fu, X. Tuning Alginate-Gelatin Bioink Properties by Varying Solvent and Their Impact on Stem Cell Behavior. *Sci Rep* **2018**, *8*, 8020, doi:10.1038/s41598-018-26407-3.
59. Noh, I.; Kim, N.; Tran, H.N.; Lee, J.; Lee, C. 3D printable hyaluronic acid-based hydrogel for its potential application as a bioink in tissue engineering. *Biomaterials research* **2019**, *23*, 3.
60. Naomi, R.; Ridzuan, P.M.; Bahari, H. Current Insights into Collagen Type I. *Polymers (Basel)* **2021**, *13*, doi:10.3390/polym13162642.
61. Iviglia, G.; Cassinelli, C.; Torre, E.; Baino, F.; Morra, M.; Vitale-Brovarone, C. Novel bioceramic-reinforced hydrogel for alveolar bone regeneration. *Acta Biomaterialia* **2016**, *44*, 97-109, doi:https://doi.org/10.1016/j.actbio.2016.08.012.
62. Fischer, L.; Nosratlo, M.; Hast, K.; Karakaya, E.; Ströhlein, N.; Esser, T.U.; Gerum, R.; Richter, S.; Engel, F.B.; Detsch, R.; et al. Calcium supplementation of bioinks reduces shear stress-induced cell damage during bioprinting. *Biofabrication* **2022**, *14*, 045005, doi:10.1088/1758-5090/ac84af.
63. Du, L.; Qin, C.; Zhang, H.; Han, F.; Xue, J.; Wang, Y.; Wu, J.; Xiao, Y.; Huan, Z.; Wu, C. Multicellular Bioprinting of Biomimetic Inks for Tendon-to-Bone Regeneration. *Advanced Science* **2023**, *10*, 2301309, doi:https://doi.org/10.1002/advs.202301309.
64. Fideles, S.O.M.; Ortiz, A.C.; Assis, A.F.; Duarte, M.J.; Oliveira, F.S.; Passos, G.A.; Beloti, M.M.; Rosa, A.L. Effect of cell source and osteoblast differentiation on gene expression profiles of mesenchymal stem cells derived from bone marrow or adipose tissue. *J Cell Biochem* **2019**, *120*, 11842-11852, doi:10.1002/jcb.28463.
65. Kriegel, A.; Schlosser, C.; Habeck, T.; Dahmen, C.; Götz, H.; Clauder, F.; Armbruster, F.P.; Baranowski, A.; Drees, P.; Rommens, P.M.; et al. Bone Sialoprotein Immobilized in Collagen Type I Enhances Bone Regeneration In vitro and In vivo. *Int J Bioprint* **2022**, *8*, 591, doi:10.18063/ijb.v8i3.591.
66. Kriegel, A.; Langendorf, E.; Kottmann, V.; Kämmerer, P.W.; Armbruster, F.P.; Wiesmann-Imilowski, N.; Baranowski, A.; Gercek, E.; Drees, P.; Rommens, P.M.; et al. Bone Sialoprotein Immobilized in Collagen Type I Enhances Angiogenesis In Vitro and In Ovo. *Polymers* **2023**, *15*, 1007.
67. Ogata, Y. Bone sialoprotein and its transcriptional regulatory mechanism. *Journal of Periodontal Research* **2008**, *43*, 127-135, doi:https://doi.org/10.1111/j.1600-0765.2007.01014.x.
68. Van der Heide, D.; Hatt, L.P.; Della Bella, E.; Hangartner, A.; Lackington, W.A.; Yuan, H.; De Groot-Barrère, F.; Stoddart, M.J.; D'Este, M. Characterization and biological evaluation of 3D printed composite ink consisting of collagen, hyaluronic acid and calcium phosphate for bone regeneration. *Carbohydrate Polymer Technologies and Applications* **2024**, *7*, 100518, doi:https://doi.org/10.1016/j.carpta.2024.100518.
69. Singh, A.; Gill, G.; Kaur, H.; Amhmed, M.; Jakhu, H. Role of osteopontin in bone remodeling and orthodontic tooth movement: a review. *Progress in Orthodontics* **2018**, *19*, doi:10.1186/s40510-018-0216-2.
70. Liu, B.; Li, J.; Lei, X.; Cheng, P.; Song, Y.; Gao, Y.; Hu, J.; Wang, C.; Zhang, S.; Li, D.; et al. 3D-bioprinted functional and biomimetic hydrogel scaffolds incorporated with nanosilicates to promote bone healing in rat calvarial defect model. *Materials Science and Engineering: C* **2020**, *112*, 110905, doi:https://doi.org/10.1016/j.msec.2020.110905.
71. Viguet-Carrin, S.; Garnero, P.; Delmas, P.D. The role of collagen in bone strength. *Osteoporos Int* **2006**, *17*, 319-336, doi:10.1007/s00198-005-2035-9.
72. Gromolak, S.; Krawczenko, A.; Antończyk, A.; Buczak, K.; Kiełbowicz, Z.; Klimczak, A. Biological Characteristics and Osteogenic Differentiation of Ovine Bone Marrow Derived Mesenchymal Stem Cells Stimulated with FGF-2 and BMP-2. *Int J Mol Sci* **2020**, *21*, doi:10.3390/ijms21249726.
73. Strassburg, S.; Richardson, S.M.; Freemont, A.J.; Hoyland, J.A. Co-culture induces mesenchymal stem cell differentiation and modulation of the degenerate human nucleus pulposus cell phenotype. *Regen Med* **2010**, *5*, 701-711, doi:10.2217/rme.10.59.

74. Senior, J.J.; Cooke, M.E.; Grover, L.M.; Smith, A.M. Fabrication of Complex Hydrogel Structures Using Suspended Layer Additive Manufacturing (SLAM). *Advanced Functional Materials* **2019**, *29*, 1904845, doi:https://doi.org/10.1002/adfm.201904845.
75. Moxon, S.R.; Cooke, M.E.; Cox, S.C.; Snow, M.; Jeys, L.; Jones, S.W.; Smith, A.M.; Grover, L.M. Suspended Manufacture of Biological Structures. *Advanced Materials* **2017**, *29*, 1605594, doi:https://doi.org/10.1002/adma.201605594.
76. Minogue, B.M.; Richardson, S.M.; Zeef, L.A.; Freemont, A.J.; Hoyland, J.A. Characterization of the human nucleus pulposus cell phenotype and evaluation of novel marker gene expression to define adult stem cell differentiation. *Arthritis Rheum* **2010**, *62*, 3695-3705, doi:10.1002/art.27710.
77. Minogue, B.M.; Richardson, S.M.; Zeef, L.A.; Freemont, A.J.; Hoyland, J.A. Transcriptional profiling of bovine intervertebral disc cells: implications for identification of normal and degenerate human intervertebral disc cell phenotypes. *Arthritis Res Ther* **2010**, *12*, R22, doi:10.1186/ar2929.
78. Livak, K.J.; Schmittgen, T.D. Analysis of Relative Gene Expression Data Using Real-Time Quantitative PCR and the 2−ΔΔCT Method. *Methods* **2001**, *25*, 402-408, doi:https://doi.org/10.1006/meth.2001.1262.